Biotribology 17 (2019) 49–63

Contents lists available at ScienceDirect

Biotribology

journal homepage: www.elsevier.com/locate/biotri

The role of denatured synovial fluid proteins in the lubrication of artificial joints

Stevenson H.[a], Jaggard M.[b], Akhbari P.[b], Vaghela U.[b], Gupte C.[b], Cann P.[a,*]

[a] Tribology Group Department of Mechanical Engineering, Imperial College London, United Kingdom
[b] Musculoskeletal Laboratory, Imperial College London, United Kingdom

ARTICLE INFO

Keywords:
Human synovial fluid
CoCrMo
Friction
Wear
Artificial hip joints, β-sheet fibrils

ABSTRACT

CoCrMo ball-on-flat wear tests were carried out with 25 wt% bovine calf serum (25BCS) and human synovial fluid (HSF) to investigate artificial joint lubricating mechanisms. Post-test the wear scar on the disc was measured and surface deposits in and around the rubbed region were analysed by Micro InfraRed Reflection Absorption Spectroscopy (Micro-IRRAS).

In most tests the HSF samples gave higher wear than the 25BCS solution; in some cases, up to 77%. After rinsing a similar pattern of surface deposits was observed in and around the wear scar for both the model and HSF. Micro-IRRAS showed the deposits were primarily denatured proteins with an increased β-sheet content. In some cases, trans-alkyl chain/carbonyl components were also present and these were assigned to lipids. Thioflavin T fluorescent imaging also indicated aggregated non-native β-sheet fibrils were present in the deposits and their presence was associated with lower wear. The formation of insoluble, denatured protein films is thought to be the primary lubrication mechanism contributing to surface protection during rubbing.

From this and earlier work we suggest inlet shear induces denaturing of proteins resulting in the formation of non-native β-sheet aggregates. This material is entrained into the contact region where it forms the lubricating film. Patient synovial fluid chemistry appears to influence wear, at least in the bench test, and thus could contributes to increased risk of failure, or success, with metal-metal hips. Finally using 25BCS as a reference screening fluid gives an overly optimistic view of wear in these systems.

1. Synovial fluid lubrication mechanisms in prothetic joints

Prosthetic joints (hips, knees etc) are lubricated by synovial fluid (SF) which fills and is replenished within the implant cavity post-operatively. SF is required to reduce friction and wear of the joint by forming a protective lubricant film over the gait cycle and under load. The properties of this film (thickness, shear strength, adherence) will significantly influence the performance and operational life of the joint. The mechanism of film formation, for example whether it is generated by isoelastohydrodynamic (i-EHL) action [1] or molecules adsorbed at the interfaces [2] will determine the ability of SF to protect the joint surfaces. Until recently most studies of joint tribology have used classical lubrication regimes to describe film formation mechanisms and predict performance under different gait conditions [1]. However, knowledge gained from engineering components lubricated with hydrocarbon oils and *a priori* extending this to biological systems is questionable. Therefore, it has significant implications for the safe development of new joint designs. For example, do SF lubricating mechanisms obey classical i-EHL film predictions over the entire joint load and speed range? If not under what conditions does the model breakdown and what are the implications for implant wear? And importantly, does patient SF chemistry play a role in determining wear and risk of failure?

More recent work in our group has considered fundamental mechanisms of SF lubrication in metal-on-metal hip joints [3–5] and in laboratory tests have shown they are more complex than earlier work has suggested. Lubricant film thickness measurements with bovine calf serum in a sliding contact have demonstrated much thicker films, under some conditions, than predicted by i-EHL equations. This is attributed to the formation of high-viscosity material due to aggregation of proteins in the inlet region [5]. However, at high sliding speeds (~ 30 mm/s), these films tend to break down [5]. Other research groups have also reported similar complex film formation behaviour with BCS lubricants [6,7].

The work has shown film formation is not determined by the bulk properties of the fluid; for example viscosity, but that the SF chemistry

* Corresponding author.
E-mail address: p.cann@imperial.ac.uk (P. Cann).

https://doi.org/10.1016/j.biotri.2019.03.003
Received 16 November 2018; Received in revised form 20 February 2019; Accepted 6 March 2019
Available online 07 March 2019

Table 1
Wear test conditions.

Test conditions	
Max Hertzian pressure	200 MPa
Frequency	20 Hz
Stroke length	1 mm
Temperature	37 °C
Duration	72,000 cycles
Test Specimens	
Material	CoCrMo Co (base), Cr (26–29%), Mo (4.5–6%), C (0.20–0.35%) and Ni (2–3%)
Ball	19.05 mm diameter
Disc	10 mm diameter

plays an important role. SF has a complex composition including proteins, lipids, and glycoproteins such as hyaluronic acid [8]. The proteins, mainly albumin and globulin are the most abundant species typically in the range 18–30 mg/ml depending on patient pathology [8]. Bovine calf serum (25 wt%, 25BCS) is usually used as a screening test fluid to replace human samples. Although there are significant differences in the chemical composition (low phospholipids, albumin/globulin ratio) the total protein content is comparable to healthy SF. The recognition that patient SF chemistry could influence implant wear and hence risk of failure is an important concept which might contribute to more effective patient screening and choice of implant materials.

There have been a number of studies reporting surface film formation on implant materials both from hip simulator and explanted specimens [9–15]. Generally two different types of film have been reported; these are proteins or glycoproteins [9,12,13] and phospholipids [10,11].

Thick, organic deposits on implant surfaces have been reported for simulator and explant hip joints [12–14]. These deposits have been identified as denatured proteins and are considered to act as solid boundary films which act to protect the sliding surfaces and reduce wear [13]. One mechanism suggested to explain deposit formation is that proteins denature due to the higher temperatures generated within the contact zone during rubbing particularly in MoP joints [13]. Roba et al. [9] identified glycoprotein (including lubricin) adsorption at the surface, as the primary friction-reducing molecules in SF.

Phospholipids are present in SF and form structured layers at the surface of biological membranes. Hills and co-workers [10] analysed surface material from a series of MoP implants using a specific solvent extraction method to remove the phospholipids. The results showed eight different types of phosphatidylcholines to be present with the unsaturated molecules being the most predominant [10]. Several studies have suggested these phospholipids act as boundary lubricants for biological and artificial surfaces [2,10].

More recently Liao et al. [15] presented experimental evidence of the formation of “graphitised” carbon films on explanted metal-metal hips joints which they suggested acted as the primary lubricant preventing wear and reducing friction.

In conclusion although a number of different chemical components have been identified on the surface of explanted hips their role in the lubrication process is still unclear, this is one of the questions addressed in this paper and as well as comparing film formation by model and HSF. In addition, in this study we have used CoCrMo as the joint material. Although the use of metal-metal hips has declined dramatically in recent years due to high failure rates some studies [16] have suggested the outcome can be good and we consider this warrants further study.

In an earlier paper [17] we compared wear properties of human and model SF solutions in a CoCrMo wear test. Post-test the average wear depth (AWD) of the scar on the disc was measured and surface deposits on the ball were observed and analysed by Micro-IRRAS. In most cases the human SF (HSF) wear was significantly greater than the 25 wt% bovine calf serum (25BCS), which was used as a reference SF. The deposits were primarily proteins [17] with a non-native β-sheet structure. To investigate this further a fluorescent method using ThT molecular dye was used to image the denatured proteins. The formation of adherent, high viscosity protein lubricant films is linked in our research to reduced CoCrMo wear [3–5]. The current paper follows on from this work by examining in more detail deposited film formation for BCS and HSF samples.

The research programme was as follows:

a. CoCrMo wear tests with 25BCS and HSF samples.
b. Post-test organic surface deposits were analysed by optical microscopy and Micro InfraRed Reflection Absorption Spectroscopy (Micro-IRRAS) which provides information on organic composition and protein structures.
c. Fluorescent imaging of deposited films by Thioflavin T (ThT), used to identify non-native β-sheet structures.
d. Scanning Electron Miscroscopy (SEM) imaging of deposited proteins in the wear scar.

These techniques are described in more detail in the next section.

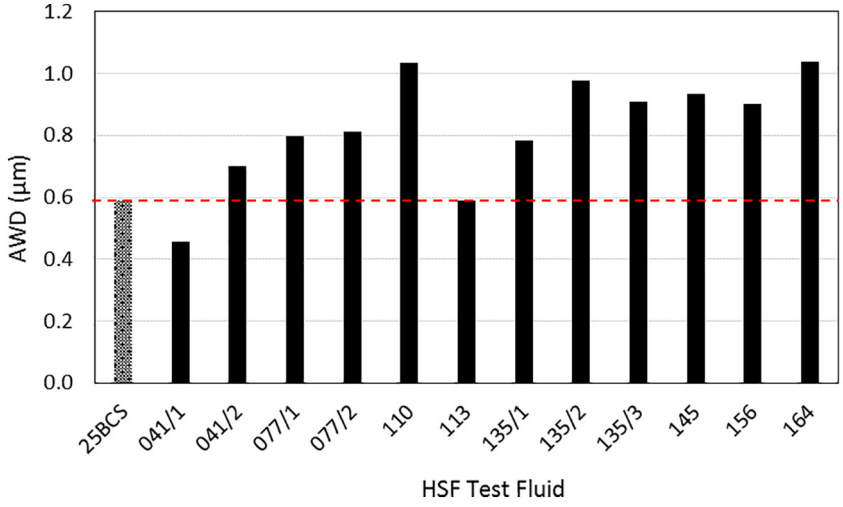

Fig. 1. Summary of average wear scar depths on disc for 25BCS and HSF (not containing ThT) tests. The 25BCS level is marked by a dotted line.

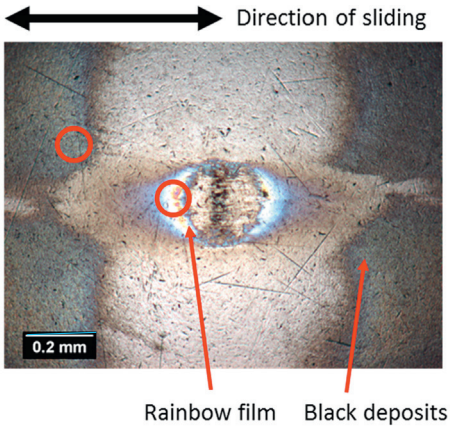

(a) An image of the wear scar and deposits on a CoCrMo ball for 25BCS test. The Micro-IRRAS sampling regions are indicated by red circles. Scale marker: 200 μm.

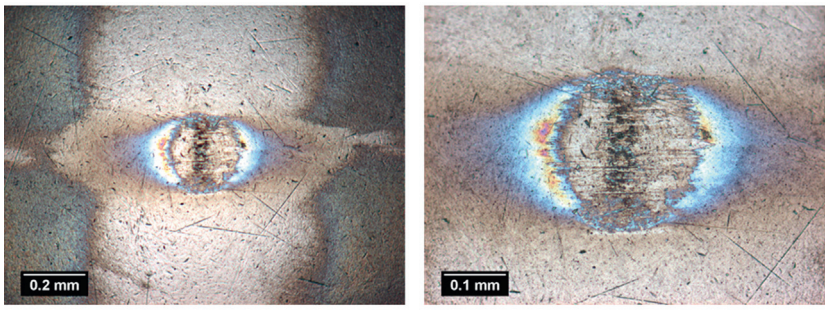

HSF077 low magnification
Scale marker: 200 μm

HSF077 high magnification
Scale marker: 100 μm

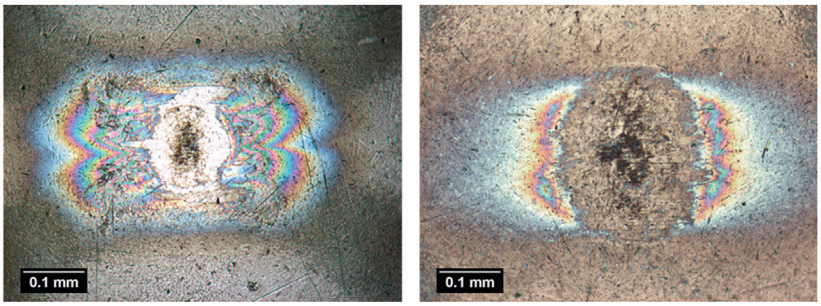

HSF145
Scale marker: 100 μm

HSF110
Scale marker: 100 μm

(b) Human SF

Fig. 2. Optical images of wear scar deposits on ball; (a) 25BCS, (b) HSF077, HSF145, HSF110.

2. Experimental procedures

2.1. Test fluids

BCS and HSF samples were tested as follows:

a. Bovine calf serum (Sigma Aldrich UK12133C sterile-filtered) as 25BCS in deionised water.
b. HSF samples with Osteoarthritis/Periprosthetic pathologies.

HSF samples were collected by MJ and his team as previously described [17]. Immediately after collection the sample is centrifuged for 15 min at 10000G to remove cellular material. Samples are divided into ~1 ml aliquots and frozen (−80 °C) until required for testing. Samples were not stored for longer than 12 months.

2.2. Wear test method

The wear test HFRR (High Frequency Reciprocating Rig, PCS Instruments, London UK) was designed to use a small amount of fluid (2 ml) allowing testing of HSF. Development of the test is reported in more detail elsewhere [17].

The test used a CoCrMo ball loaded and reciprocated against a CoCrMo disc to simulate metal-metal hip articulation. It was run with a bulk fluid temperature of 37 °C at a frequency of 20 Hz and 1 mm stroke length, which gives a mid-stroke speeds of 42 mm/s. Test duration was

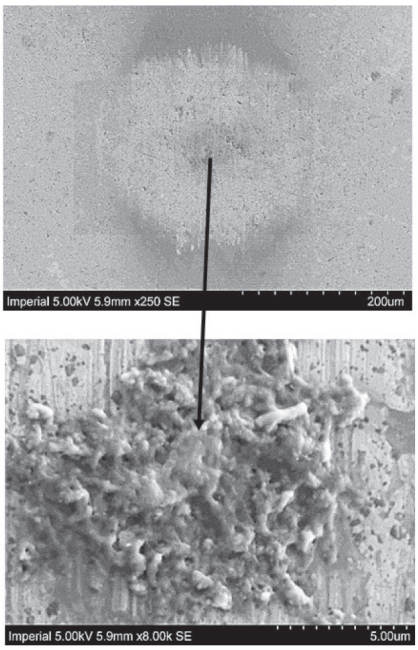

(a) Upper: overall image of wear scar on ball for a HSF test Lower: higher magnification image of deposit within the scar

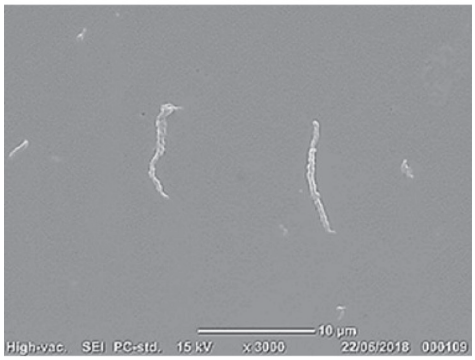

(b) Single fibrils from the disc wear scar region for a 25BCS test. Fibrils are aligned perpendicular to the sliding direction

Fig. 3. SEM images of deposits (a) from the centre of the wear scar on ball. (b) from the wear scar region on disc.

72,000 cycles. The load was 1 N giving a mean Hertz pressure of 200 MPa [17]. These conditions are summarised in Table 1.

Ball and disc CoCrMo test specimens (19.05 mm diameter ball, 10 mm diameter disc) were polished to a mirror finish (as obtained from PCS Instruments, UK) with surface roughness (rms) 39.6 ± 1.5 nm and 8.8 ± 0.8 nm respectively. Before testing the specimens were cleaned in 1% detergent solution and rinsed (3 times) in distilled water. The specimens were then stored under isopropanol. Just before testing they were air-dried and cleaned in an oxygen plasma which removes organic contamination.

A fluid sample of 2 ml was used in the tests. Bovine calf serum (Sigma Aldrich Poole, UK12133C sterile-filtered) was used as the reference test fluid. On receipt the 500 ml sample was divided into 7 ml aliquots and then refrozen and stored at −40 °C. An aliquot was removed the day before testing, defrosted overnight in a refrigerator and then diluted (deionised water) to the required concentration before testing. 25 wt% bovine calf serum (25BCS) was used as a reference test fluid this was prepared by diluting the BCS concentrate (3:1) with deionised water and mixing carefully before testing. At least 3 repeat tests were carried out with the 25BCS. The amount of HSF collected varied for each patient, however whenever possible repeat tests were carried out.

2.3. Wear measurement and imaging of surface films

At the end of the test the specimens were removed and retained for further analysis. The disc was washed with detergent solution and then rinsed with water to remove surface deposits to allow accurate measurement of the wear scar. A White Light Interferometer (WLI Wyko NT9100) was used to measure the diameter of the wear scar formed on the disc [17], images were obtained using a 20× magnification objective (at 0.55 FOV). The wear scar diameter was measured at three positions across the width and averaged (AWD). The wear results will not be reported in detail in this paper as the focus is on the film properties. Further results can be found in reference 17.

To analyse the deposits on the ball a different cleaning procedure

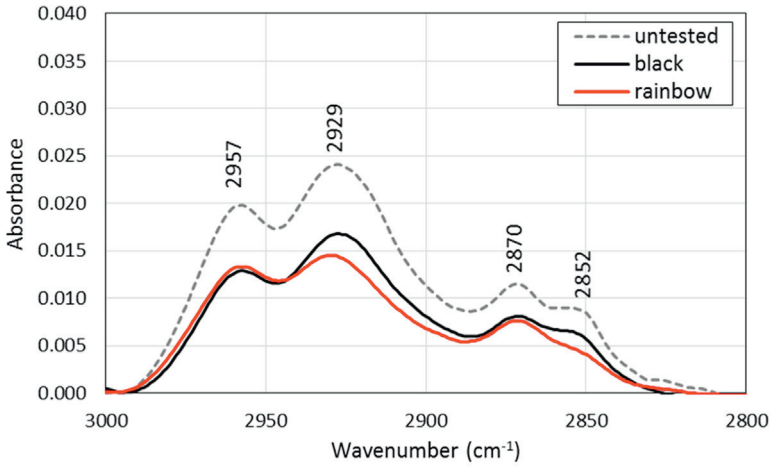

(a) 3000-2800 cm^{-1}

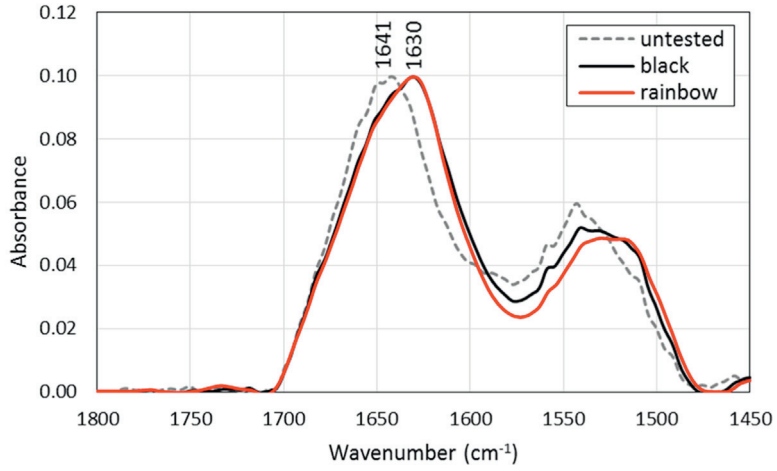

(b) 1800-1400 cm^{-1}

Fig. 4. Micro-IRRAS analysis of surface films for 25BCS (a) 3000–2800 cm^{-1} (b) 1800–1400 cm^{-1} range.

was adopted. Post-test the ball was lightly rinsed with deionised water and air dried at room temperature, which removed excess test fluid but left the tightly bound deposits. A low power microscope was used to image deposits in and around the wear scar. In some cases the deposits were analysed by a Nikon 6000 SEM.

2.4. Chemical composition: micro-IRRAS and thioflavin T fluorescent imaging

Micro-IRRAS was used to examine the organic composition of the surface deposits. The technique has been used extensively to provide information on the chemical bonding of organic lubrication films [17,18]. The surface deposits were analysed by a Perkin Elmer Multiscope Infrared Microscope coupled to a Frontier FTIR spectrometer. The spectra were compared to the untested fluid which was sampled as thin films dried on CoCrMo surfaces [17].

An aperture mounted in the microscope was used to define the sample diameter which was limited to 100 µm. The scan conditions were 100 scans and 4 cm^{-1} resolution. The resulting spectrum was baseline corrected (4000–700 cm^{-1}), smoothed (13 point) and normalised (to absorbance 0.1 at 1650 cm^{-1}) using standard Perkin Elmer software. The analysis concentrated on two spectral regions: 3000–2800 and 1800–1400 cm^{-1}, which corresponded to the CH stretch region and Amide I and II peaks respectively. Amide I bands are a mixture of C═O and N—H vibrations and have been extensively used to probe protein secondary structure, for example the presence of globular, disordered or β-sheet structures [19]. To identify peaks contributing to the broad Amide I band, 2nd derivative and deconvolution analysis of the spectra were also carried out using the Perkin Elmer software.

Thioflavin T fluorescent dye (ThT) has been used extensively to identify β-sheet proteins and in particular non-native fibrils [20,21] which have a parallel sheet structure [22,23]. In a limited number of cases fluorescent imaging was used with ThT-doped 25BCS and HSF samples (HSF108 and HSF128) tested in the HFRR. The surface deposits on the wear samples were imaged using a Navitar fluorescent microscope with an Olympus filter cube set (Chroma (435/480 nm) 49001 - ET – ECFP) and mid-blue LED all supplied by Close Ups Ltd., UK. The fluorescence protocol was as follows: 500 µM ThT (Sigma Aldrich) was prepared in deionised water. 25BCS_ThT solutions were prepared as follows: an initial solution of 500 µM ThT was made, this was then combined with 100BCS in a 3:1 ratio to give 25BCS with ThT at a

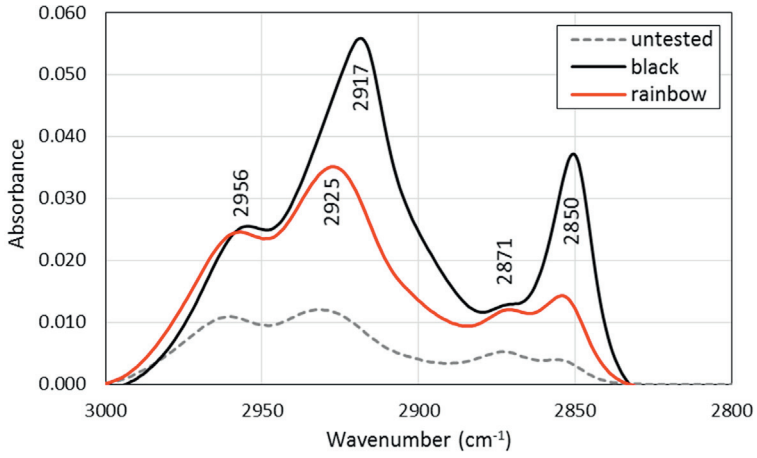

(a) 3000-2800 cm^{-1}

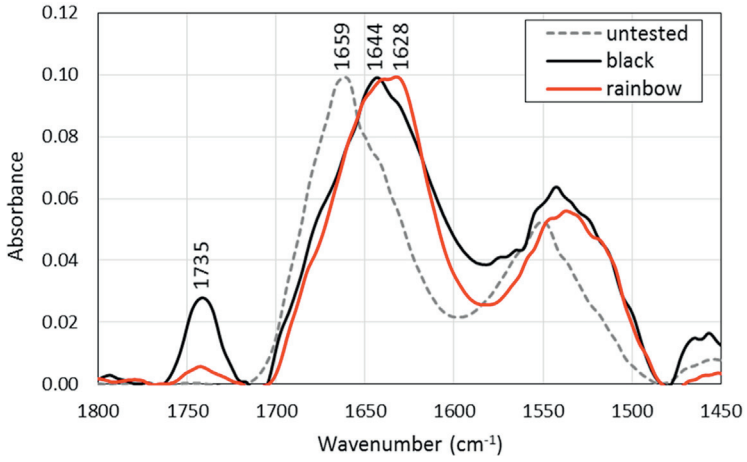

(b) 1800-1400 cm^{-1}

Fig. 5. Micro-IRRAS analysis of surface films: human HSF041 (a) 3000–2800 cm^{-1} (b) 1800–1400 cm^{-1} range.

concentration of 375 µM. Human samples were also prepared to yield ThT at the same concentration: 200 µl of a 3750 µM ThT solution was combined with the HSF sample (2 ml) to give 375 µM ThT concentration. Post-test the ball and disc specimens were drained, lightly-rinsed with water and then analysed by visual and fluorescence microscopy. The untested solutions (doped with ThT) were also examined as dried films on a CoCrMo surface [17].

In our earlier papers [5] we suggested that shear alone was sufficient to form denatured β-sheet aggregates. To explore this idea, in a limited number of tests, a small volume of 25BCS_ThT solution was manually sheared between glass microscope slides and viewed under the fluorescent microscope.

3. Results

3.1. Average wear diameter (AWD) results

AWD (where possible in some cases only single tests could be carried out on HSF samples) for all tests are plotted in Fig. 1. Repeatability of wear results for 25BCS was very good: the AWD was 0.59 µm (SD 0.047) and in most cases where repeat tests were possible this was found to be acceptable for the HSF samples. However, in the two tests for HSF041 significantly different AWD results were obtained and this was thought to be due to fractionation of the low volume samples at the initial collection. Most of the HSF samples gave larger AWDs than 25BCS, up to 77% increase and we reported similar results for an earlier set of tests [17].

Friction coefficient was recorded throughout the test however we do not report these results in detail. As before [17] all samples (25BCS, HSF) gave friction coefficients in the range µ = 0.25–0.3 and there was limited correlation with AWD values.

3.2. Optical and SEM images of wear scar deposits

Optical images from the deposits close to the wear scar on the ball are shown in Fig. 2. Fig. 2a shows a low-magnification image from a 25BCS test where the “rainbow” films and “black” deposits are clearly seen. The samples areas for the Micro-IRRAS analysis are also shown. Fig. 2b shows a selection of images from the HSF tests: one low magnification (HSF077) and three higher magnification (HSF077, HSF110, HSF145) pictures. The images for the 25BCS and human samples show similar types of film formation; in all cases the rainbow and black films are present as well as deposits in the centre of the wear scar. The rainbow deposits appear either side of the wear scar in line with sliding direction and effectively they represent the inlet/exit region of the reciprocating stroke. In general, 25BCS formed more extensive black deposits than the human samples. In many cases black, fibrillar, deposits are seen in the centre of the wear scar, for both the BCS and HSF

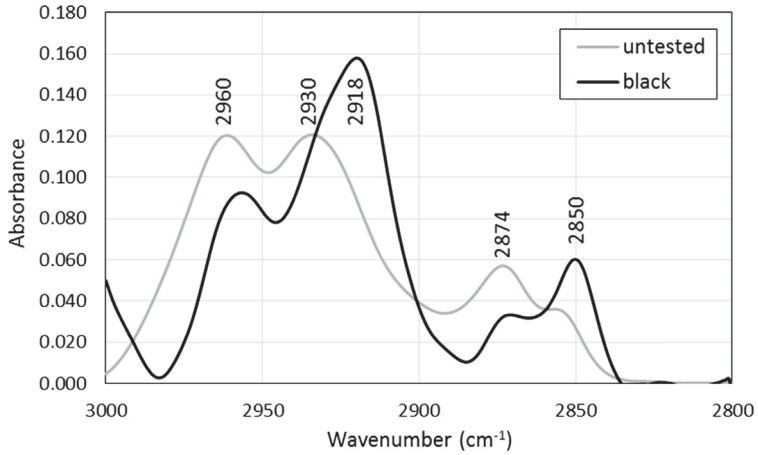

(a) 3000-2800 cm^{-1}

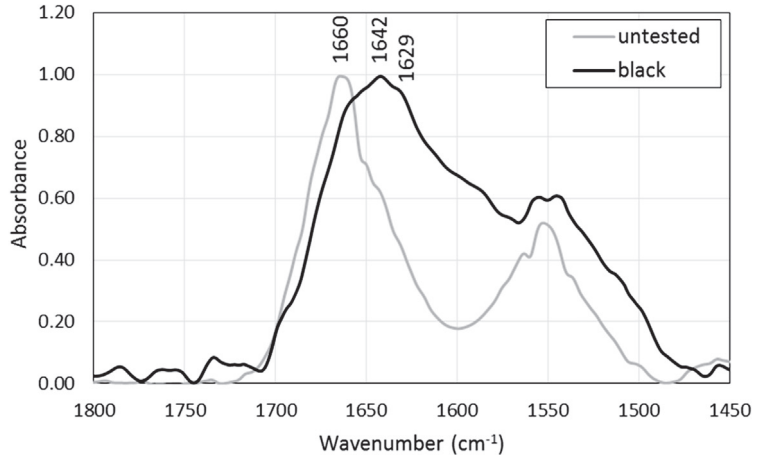

(b) 1800-1400 cm^{-1}

Fig. 6. Micro-IRRAS analysis of surface films: human HSF077 (a) 3000–2800 cm^{-1} (b) 1800–1400 cm^{-1} range.

samples.

An SEM image of a wear scar deposit from an HSF test is shown in Fig. 3a. At high magnification the deposit appears as a tangled rope structure with strands ~0.5 μm thick, which are thought to be aggregated proteins consisting of non-native β-sheets [24]. Fig. 3b shows an SEM image of single fibrils remaining in the disc wear scar region after a 25BCS test, where the twisted structure can be seen. The fibrils are generally aligned perpendicular to the sliding direction.

3.3. Micro-IRRAS spectra of surface deposits

Deposited film Micro-IRRAS spectra at different positions around the wear scar are shown In Fig. 4 for 25BCS and Figs. 5, 6 and 7 for HSF samples. Spectra of the pre-test fluid (Untested) are also shown as a comparison. Both rainbow and black films were sampled and where possible this has been identified in the spectra, however in many cases it was not possible to make a definite attribution.

The spectra are divided into two wavenumber ranges 3000–2800 cm^{-1} and 1800–1400 cm^{-1} corresponding to the CH stretch and Amide I and II regions respectively [19]. The CH stretch region provides information on the alkyl chain structure and the presence of non-protein species. All the spectra are normalised against the Amide I peak and thus a relative increase in CH stretch intensities indicates the presence of non-protein molecules or a change in the protein distribution. The Amide I band is mainly due to the C═O (~80%) stretching vibration [25–27] with contributions from the out-of-phase CN stretching vibration usually in the range 1600–1700 cm^{-1}. The Amide II peak is a combination of the NH bending (~60%) and CN stretching vibration (~40%) absorbing frequencies in the range of 1510–1580 cm^{-1} [25,26]. Amide I and II vibrations are little affected by the nature of the side chain however peak position does depend on the secondary structure of the peptide backbone [25–27]. Our analysis is limited to the Amide I band position and general ranges for different secondary structure peak assignments are summarised in Table 2.

The spectra for 25BCS are shown in Fig. 4 which includes the untested fluid and spectra from different post-test films. The untested and wear-deposit spectra in the CH stretch region are very similar with the main peaks at ~2960 (methyl, υ_{asym} CH_3) ~2932 (methylene υ_{asym} CH_2) and ~2872 (methyl υ_{sym} CH_3) cm^{-1}. A shoulder is seen at ~2850 cm^{-1} which is the υ_{sym} CH_2 (methylene) band. In most cases a decrease in CH peak intensity (relative to Amide I) was observed for the 25BCS film spectra compared to the untested fluid. The origins of this change are unclear but would suggest a relative loss of non-protein organic species or change in protein composition in the deposited BCS films.

In contrast the HSF spectra showed significant changes in the CH stretch region for the wear deposits compared to the untested fluid. In the wear-deposit spectra there is usually an increase in the υ_{asym} CH_2

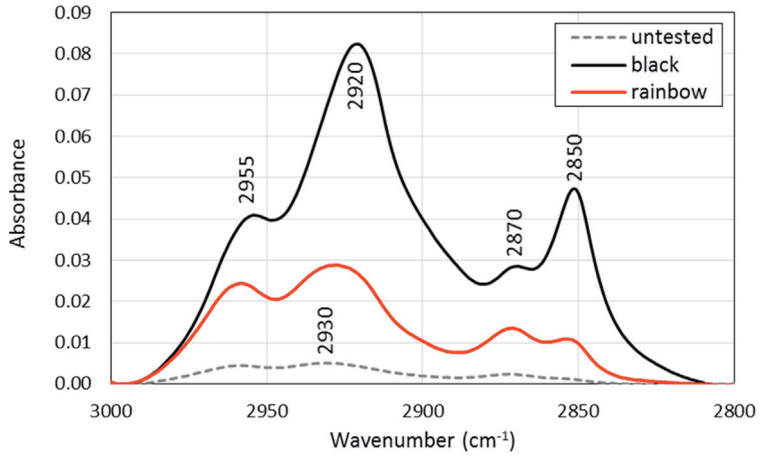

(a) 3000-2800 cm^{-1}

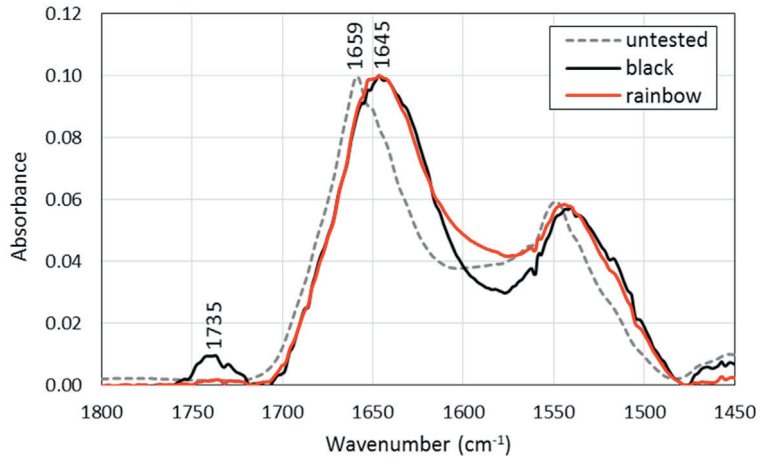

(b) 1800-1400 cm^{-1}

Fig. 7. Micro-IRRAS analysis of surface films: human HSF164 (a) 3000–2800 cm^{-1} (b) 1800–1400 cm^{-1} range.

Table 2
Amide I band positions and protein secondary structure [25–27].

Protein secondary structure	Amide I position cm^{-1}
Turns and bends	> 1660
α-helix/random coil	1660–1645
β-native protein	1641–1630
β-sheet aggregated	1700–1680
Oligomer	1640–1630
β-sheet aggregated strands	1632–1611

absorbance intensity (relative to the normalised Amide I band) accompanied by a shift to lower wavenumbers. Examples of this are seen in Figs. 5 and 7 where the υ_{asym} CH_2 absorbance increases from A = 0.012–0.015 to A = 0.055 (HSF041) and A = 0.082 (HSF164). The υ_{asym} CH_2 peak shifts typically from ~2930 cm^{-1} (untested fluid) to ~2918 cm^{-1} (wear deposit). In addition, the υ_{sym} CH_2 peak absorbance at ~2850 cm^{-1} increases, this is clearly seen in the black deposits of HSF041 (Fig. 5), HSF077 (Fig. 6) and HSF164 (Fig. 7). All of these changes are thought to be due to the presence of non-protein molecules containing unbranched trans-alkyl chains [28]. These have an ordered structure where all the alkyl groups are arranged in the trans position and are associated with phospholipids and fatty acid molecules [28]. In this case the alkyl chains have adopted a more ordered, semi-crystalline structure and as a result the IR bands are much sharper and occur at lower wavenumbers [28].

In the Amide I and II spectral region (1800–1400 cm^{-1}) differences in the pre and post-test IR spectra are seen for both the BCS and HSF fluids. The main Amide I band shifts to a lower wavenumber signifying a change in the distribution of protein secondary structures. In some cases, this behaviour is not so apparent, however it must be emphasised that the majority of post-test film spectra analysed showed significant shifts in the Amide I band for both model BCS and HSF spectra [17]. Evidence of this is seen in the HSF spectra in Figs. 5, 6 and 7 which show representative spectra from HSF041, 077 and 164 respectively. Deconvolution and 2nd derivative analyses of the spectra were carried out which allowed more accurate identification of individual peak positions within the Amide I envelope and these are summarised in Table 3. The main Amide I peaks for the BCS film spectra shifted from ~1640 cm^{-1} (predominately α-helix/random coil) to 1632–1626 cm^{-1} which is associated with an increase in the non-native β-sheet content [26,27]. For the HSF samples the main Amide I band shifted from ~1660 cm^{-1} to 1651–1642 cm^{-1} again signifying an increase in β-sheet content. In addition, minor peaks at ~1612 cm^{-1} associated with

Table 3
Summary of IR peak positions (1800–1500 cm^{-1}) (a) 25BCS (b) HSF041 (c) HSF164 (d) HSF156.

(a) 25BCS

Peaks	Untested	Black	Rainbow	Structure
Amide I	1659	1659	1659	Helical/disordered
	1651	1650	1651	Helical/disordered
	1641	1643	1643	Native β-sheet
	1632	**1632**	**1632**	β-sheet (incl. non-native)
		1612[w]	1613[w]	β-sheet aggregated strand

(b) HSF041

Bands	Untested	Black	Rainbow	Structure
C=O		1735	1735	Lipid
Amide I	1666			Turns and bends
	1659	1659	1659	Helical/disordered
	1650	1651	1651	Helical/disordered
	1642	**1644**	1640	Native β-sheet
	1632	1631	**1631**	β-sheet (incl. non-native)
		1612[w]	1612	β-sheet aggregated strand

(c) HSF077

Bond	Untested	Black	Rainbow	Structure
Amide I	1665			Turns and bends
	1660	1660		Helical/disordered
	1650	1651		Helical/disordered
	1642	**1642**		Native β-sheet
	1632	1629		β-sheet (incl. non-native)
		1613		β-sheet aggregated strand

(d) HSF164

Bands	Untested	Black	Rainbow	Structure
C=O		1735		Lipid
Amide I	1666			Turns and bends
	1659	1660	1659	Helical/disordered
	1650	**1651**	**1652**	Helical/disordered
	1643	1643	1642	Native β-sheet
	1632	1633	1630	β-sheet (incl. non-native)
		1613[w]	1612[w]	β-sheet aggregated strand

Wavenumber in **bold** indicates most intense peak. [w]weak shoulder.

β-sheet aggregated strands were identified in the wear deposits. These changes are discussed in more detail later.

3.4. ThT fluorescent imaging

Images from the HFRR samples tested with ThT-doped 25BCS and HSF are shown in Fig. 8. Fig. 8a shows optical and ThT fluorescence images from 25BCS wear deposits on the ball. The bright regions around the wear scar correspond to the black deposits seen in the upper image and are indicative of β-sheet fibril proteins. The rainbow deposits close to the wear scar are also visible although the intensity is relatively reduced. Within the wear scar bright individual "rope" forms are observed.

Similar images are shown for HSF108 and 163 in Fig. 8b. These were carried out as a separate series of tests as the samples contained ThT and the wear rankings are summarised in Fig. 9a. The associated Amide I spectra for 25BCS, HSF108 and HSF163 wear deposits are shown in Fig. 9b.

HSF108 gave the lowest AWD (0.25 μm) of all human fluids tested and HSF163 close to the highest (1.1 μm). Clear differences are seen in the upper optical microscope images of the wear deposits for the two fluids. The more intense interference colours with multiple orders visible indicate HS108 formed much thicker rainbow deposits than HSF163. The fluorescence image for HSF108 clearly shows the rainbow deposits with many bright fibrils within the films. In addition bright "roll" deposits can be seen in the wear scar. HSF163 shows a slight overall increase in fluorescence indicating higher viscosity deposits [29] although some brighter fibrils are seen.

The Micro-IRRAS spectra also show differences between the low AWD (HSF108) and high AWD (HSF163) samples. The wear deposit primary Amide I band for HSF108 occurs at 1632 cm^{-1} (β-sheet non-native) with a minor peak at 1612 cm^{-1} which is assigned to aggregated strands. This is similar to the result for 25BCS. The high AWD HSF128 had a primary Amide I peak at 1640 cm^{-1} indicating a more native β-sheet film.

4. Discussion

Wear tests were carried out for model (BCS) and HSF samples; in most cases the AWD was higher (up to 77%) [17] for the human samples compared to the 25BCS reference fluid. Post-test organic deposits on the ball were analysed by Micro-IRRAS and in some cases ThT fluorescent imaging. Micro-IRRAS confirmed earlier results [17] which showed the formation of protein deposits with an increased β-sheet content for both the 25BCS and HSF specimens. Interestingly the deposits, particularly the thick black regions, were much less for the HSF tests compared to 25BCS. If β-sheet formation in the lubricating film does protect against surface wear then this observation helps to explain why 25BCS gives lower AWD than most of the HSF samples.

The conclusion that non-native β-sheet-rich deposits are formed was confirmed by ThT fluorescent imaging, however the interpretation of these results is not straightforward. ThT is also used as a fluorescent agent to indicate high viscosity solvents [29]. Thus, two interpretations of the fluorescent response are possible, and complementary, as we suggest during rubbing proteins denature forming insoluble, high viscosity, β-sheet aggregates. In the following sections we examine in more detail protein structure changes, interpretation of the FTIR spectra and the implications of the ThT results.

4.1. Protein secondary structure and β-sheet formation

One of the key findings is that deposits have an increased β-sheet content, and in some cases non-native structures are formed. It is useful at this point to review in more detail protein secondary structures and the implications of these findings.

Proteins are high molecular weight polypeptide chains formed from amino acid molecules with a characteristic structural hierarchy primarily driven by H-bonding and non-hydrophobic interactions. In natively folded proteins they are mainly α-helix and native β-sheet structures formed by H-bonding between oxygen and NH groups on the peptide backbone. Further ordering occurs as the α-helices and native β-sheet form globular structures through shielding of hydrophobic groups from water [30]. Disruption of the native fold structure can occur forming denatured proteins which may aggregate to form soluble oligomers [31] or insoluble fibrils [32] both with a high β-sheet content. Extended polypeptide chains are held together by intermolecular H-bonding where two structures are possible: parallel (fibril) and antiparallel (oligomer) depending on the arrangement of the peptide chains. Fibril structures are formed by pleated cross β-sheets which aggregate by entwining to form a coiled rope-like form [24,33]. SEM images of HSF and 25 BCS deposits in the wear scar also showed this type of structure (Fig. 3). Misfolding of proteins to form insoluble deposits can be caused by a number of factors including chemical (pH, ionic strength) or physical [high pressure, high temperature, shear) cell environments [23].

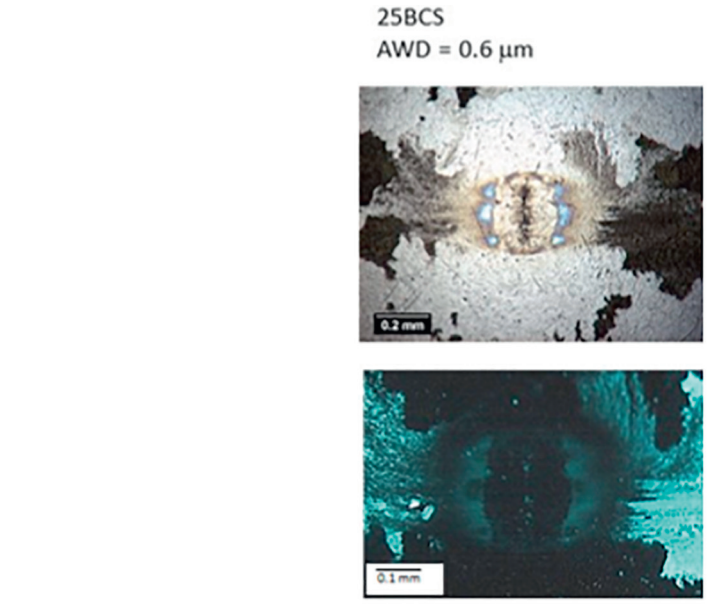

Fig. 8. Optical (upper) and ThT fluorescent (lower) imaging of deposited films around the ball wear scar for (a) 25BCS and (b) HSF samples. The bright blue regions in the lower images indicate β-sheet rich proteins. (For interpretation of the references to colour in this figure legend, the reader is referred to the web version of this article.)

4.2. Interpretation of micro-IRRAS Spectra

Several studies [31,32,34–36] have reported using Amide I IR bands to distinguish between native β-sheet proteins and the aggregated oligomer and insoluble fibril structures. Zandomeneghi et al. [32] in their review of the literature reported broad spectral ranges for the Amide I band of 1643–1630 cm^{-1} for the native β-sheet proteins and 1630–1611 cm^{-1} for β-sheet fibrils. Cerf et al. [31] also reported fibrils had a parallel β-sheet conformation which was associated with a strong band at 1630 cm^{-1}. The soluble oligomeric form with an antiparallel β-sheet structure had IR bands in the Amide I region at ~ 1630 cm^{-1} (strong) and a much weaker component at 1695 cm^{-1}. Ami et al. [34] reported similar results in their study of amyloid fibrils in tissue of patients affected by systemic light chain (LC) amyloidosis. For the *in vitro* amyloid β-sheet the main Amide I peak shifted to a lower wavenumber, typically at 1629 cm^{-1}. Analysis of *ex vivo* amyloid fibres from heart tissue also showed the main Amide I peak at ~ 1630 cm^{-1}. They concluded the "*~ 1630 cm^{-1}band can be considered a marker of amyloid aggregates in tissues*" [31] Other studies [35,36] have shown fibril Amide I bands absorbing at lower wavenumber ~ 1620–1612 cm^{-1} and in some cases there is an additional peak above 1680 cm^{-1} [35]. In studies of amyloid-like nanofibrils in barnacle cement parallel β-sheet fibril structures are reported to have Amide peaks in the range ~1620–1610 cm^{-1} [36].

In this study differences were observed in the untested 25BCS and HSF samples as well as in the post-test films. Representative spectra for untested fluids are compared in Fig. 10 for 25BCS and HSF (HSF164). The corresponding Micro-IRRAS spectra for the wear scar deposits are

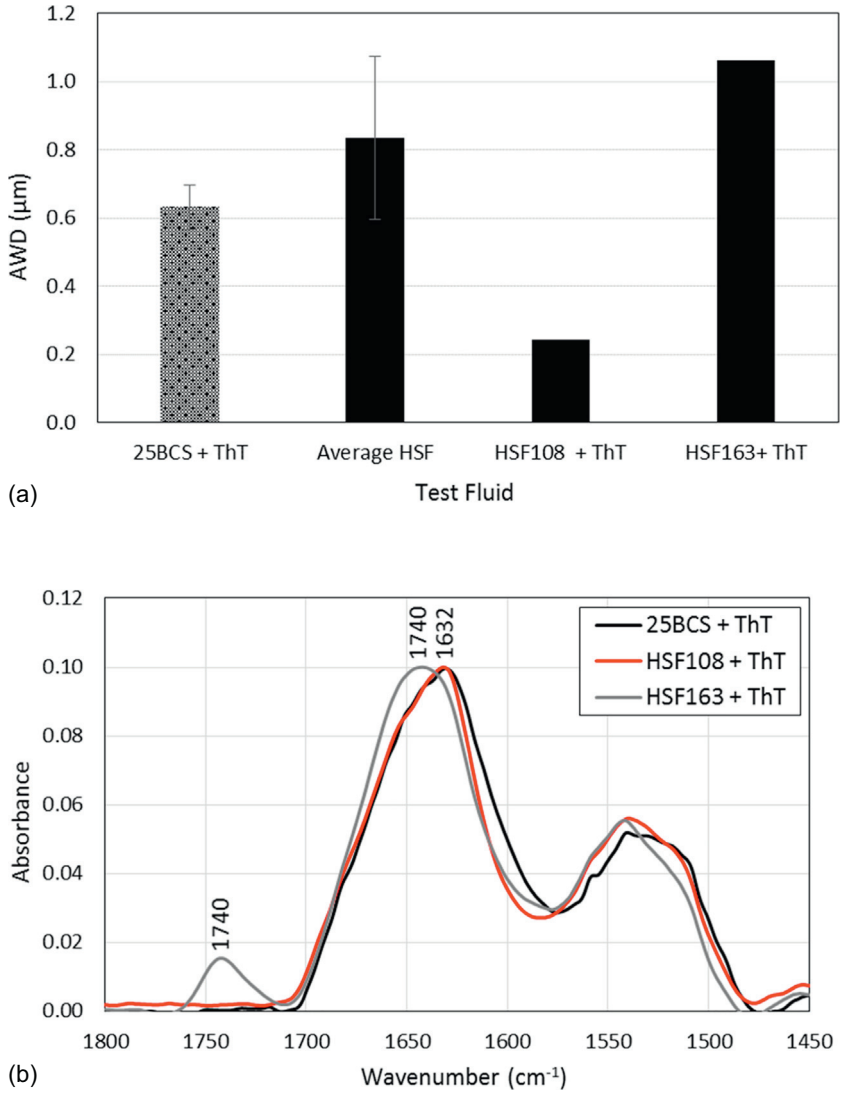

Fig. 9. (a) Summary of AWD for wear tests with ThT-doped fluids and comparison with average AWD(HSF-AV) for all HSF fluids (non-ThT-doped) (b) Comparison of Amide I peak region for post-test deposits with ThT-doped fluids.

compared in Fig. 11. Overall the Amide I band occurs at higher wavenumbers for the untested HSF samples compared to the 25BCS fluid indicating a more predominant α-helix content.

For the wear deposit analysis: with 25BCS the main Amide I band shifts to a lower wavenumber (~1630 cm^{-1}) compared to most HSF (~1640 cm^{-1}) samples (Fig. 11). However, deconvolution analysis of the HSF film spectra also shows a component at ~1630 cm^{-1} (Table 4) suggesting non-native structures are present. In addition, minor peaks at ~1612 cm^{-1} are identified for 25BCS and these are assigned to aggregated strands. These results suggest that BCS forms insoluble deposits with greater non-native β-sheet content. HSF forms films with some aggregated β-sheet strands but the main component is β-sheet native proteins. The exception was HSF108 which gave a very low AWD value and had Amide I peaks at 1632 and 1612 cm^{-1}, which are indicative of β-sheet aggregated strands.

One of the most interesting aspects of the FTIR spectra is the peak changes in the CH stretch region. In many of the HSF wear deposit spectra the CH stretch peaks increased in intensity compared to the untested fluid (Figs. 5a, 6a and 7a) and the dominant peaks are shifted to lower wavenumbers at ~2918 and 2850 cm^{-1}. This indicates higher non-protein content, as the spectra are normalised to Amide I band, and an increased proportion of trans-alkyl chain components [28]. These changes were often accompanied by a new band at ~ 1735 cm^{-1} assigned to a C═O band (Figs. 5b and 7b). Our conclusion from these observations is that lipids in HSF, are present in the deposited films. These spectral features are not observed in the untested fluids (Fig. 10) which suggest they are present in much higher concentrations in the wear deposits (Fig. 11). We suggest the lipids play an active role in the lubrication process and appear to inhibit non-native fibril β-sheet formation thus contributing to an increased AWD. These changes in the CH stretch peaks were not found to the same extent in the 25BCS spectra. For example, the peak positions remain the same but a decrease in overall CH peak intensity (relative to the untested fluid) is seen for the wear scar films in Fig. 4 possibly indicating a change in the overall protein profile.

4.3. ThT fluorescence and β-sheet formation

The Micro-IRRAS evidence confirms the formation of insoluble deposits with an increased β-sheet content for both 25BCS and HSF samples. One key question is whether these deposits have a parallel or anti-parallel sheet structure. Parallel β-sheet structures are associated with amyloid-type fibril formation, anti-parallel with oligomer aggregate formation [31, 35] although the latter have also been related to subsequent amyloid formation [31, 35, 37].

ThT fluorescence is reported to be specific to cross β-sheet fibrils

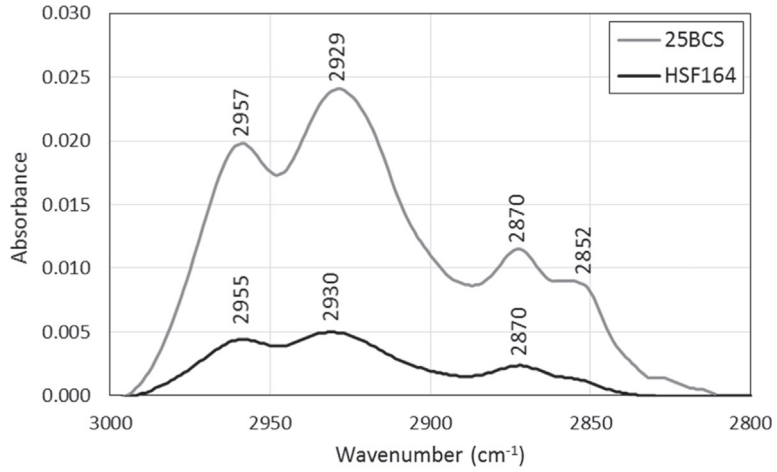

(a) 3000-2800 cm^{-1}

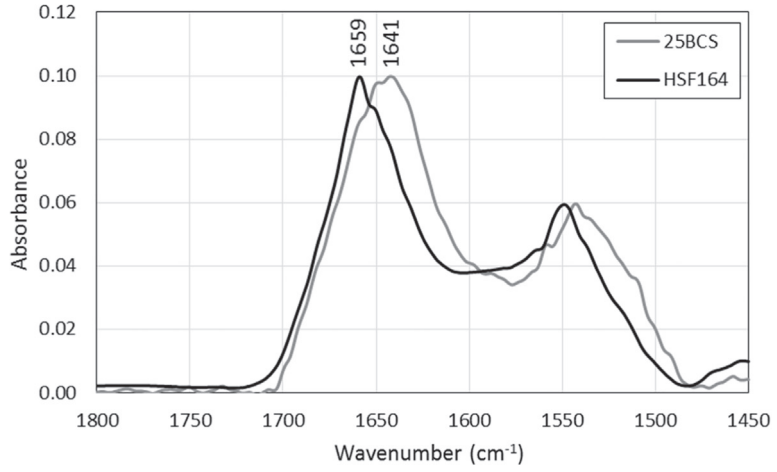

(b) 1800-1400 cm^{-1}

Fig. 10. Comparison of Micro-IRRAS spectra for untested fluids 25BCS and HSF 164.

and insensitive to native β-sheet domains [20–22]. LeVine III [20] showed for a range of native proteins (β, αβ) including serum albumin did not induce fluorescence and concluded "*only the multimeric fibrillary forms of the β-sheet polymers, not β-sheet monomers or oligomers, fluoresce with ThT*". He also suggested the requirement was for "*stacked cross β-pleated sheet structures*" which was why the β-sheet domains in native proteins did not fluoresce. Similarly, Malmosa et al. [22] state *"ThT with amyloid fibrils is highly specific. Neither amorphous aggregates nor soluble proteins in folded, unfolded, or partially folded states enhance ThT fluorescence"*.

In our work ThT samples were imaged as thin films before testing to check fluorescent components were absent. In all cases only isolated fluorescent particles were observed and in the most part the images were completely dark. In addition, the wear test run with ThT solution alone did not produce fluorescent deposits.

The ThT-doped images in Fig. 8 show fluorescent deposits around the wear scar corresponding to the areas of denatured proteins identified by Micro-IRRAS. The fluorescence for the 25BCS test was particularly intense (Fig. 8a). Fig. 8b also shows ThT fluorescent deposits around the wear scar for two HSF samples where fibril structures can also be seen. Isolated bright fluorescent "coil" deposits are seen in the wear scar possibly indicating entangled fibres forming a rope structure which is also shown in the SEM image (Fig. 3). In Fig. 8 the weaker "background" fluorescence is possibly due to the intrinsically high viscosity of the deposit [29].

In earlier papers [3–5] we suggested that shear, rather than thermal effects [13] could be responsible for protein denaturing and aggregation. This idea is supported by the image shown in Fig. 12 which shows fluorescent fibril-like structures formed during simple shearing of 25BCS between glass slides, the arrow indicates the primary direction of sliding. These structures form very rapidly; within a few strokes and have been obtained with both 25BCS and HSF samples. In all cases they initially form perpendicular to the direction of sliding, if cross shear is imposed, they start to agglomerate to give larger structures. There are many studies [23,38–42] reporting β-sheet fibril formation due to shear for a range of protein solutions including β-lactoglobulin [38]. These generally conclude that shear promotes amyloid fibril formation due to unfolding of protein structure exposing the hydrophobic core followed by lateral aggregation of the polypetide chains [39].

In the images of post-test deposits two types of film are observed: black particulate/fibrillar deposits and amorphous rainbow-coloured films. We suggest the different appearance of these films can be explained by a combination of shearing and thermal effects. The lubricating film in the sliding contact is formed by fluid sheared in the converging inlet. In addition, excess fluid is sheared as it flows around the contact in the confined gap ball-on-flat geometry. In both regions

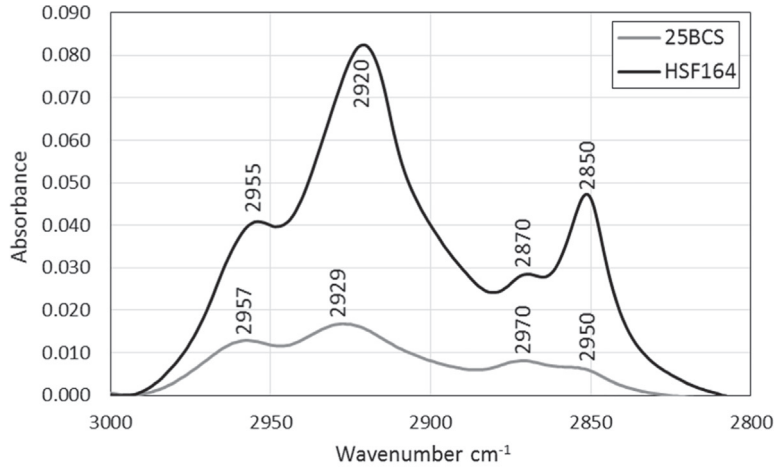

(a) 3000-2800 cm^{-1}

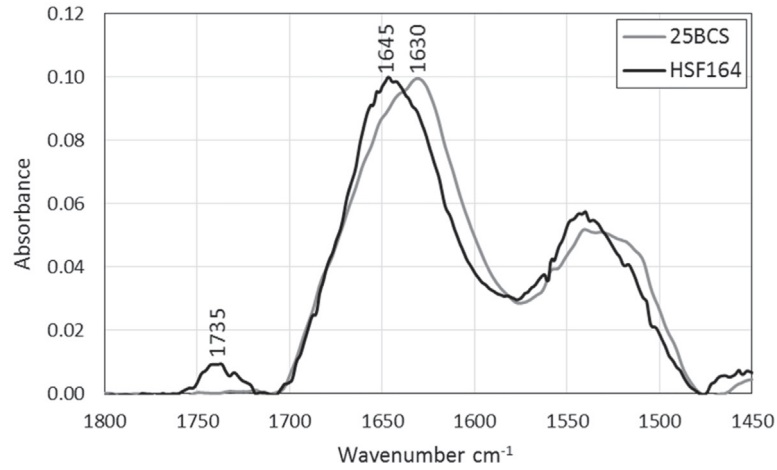

(b) 1800-1400 cm^{-1}

Fig. 11. Comparison of Micro-IRRAS spectra for wear scar deposits for 25BCS and HSF 164.

Table 4
Summary of FTIR Amide I peak positions for ThT tested fluids.

Bond	25BCS	HSF108	HSF163	Structure
Amide I	1659	1659	1660	Helical/disordered
	1650	1639	1650	Helical/disordered
	1643	1640	**1640**	Native β-sheet
	1632	**1632**	1632	β-sheet (incl. non-native)
	1612 [w]	1612 [w]		β-sheet aggregated strand

Wavenumber in **bold** indicates most intense peak. [w]: weak shoulder.

globular proteins will be distorted in the shear flow forming extended chains exposing the hydrophobic cores [39]. In a confined gap these form intermolecular H-bonds so that further interaction to generate aggregated, insoluble β-sheets could occur; this is the origin of the black, fibrillar material deposited around the contact. Measurements from images on the balls indicate that the black deposits extend from the end of the rainbow deposit at a gap height ranging from 4.8–13.7 μm and extend outside the view of the image indicating the black deposits formed at gaps larger than 22 μm. Very simple calculations would indicate shear rates of the order of 10^3–$10^4\,s^{-1}$ in this region rather than 10^7–$10^8\,s^{-1}$ normally associated with the inlet region. By dropping out of solution onto the CoCrMo surface the denatured proteins do not experience the much higher shear rates in the bulk fluid close to the contact. If this material is formed on the moving surface in the inlet region it is entrained into the contact where it contributes to lubricant film formation and surface separation. Friction in the contact zone would generate local temperature rises which could transform the fibrils into a high-viscosity gel [43] This would explain why the amorphous "rainbow" films are seen on either side of the contact in the inlet/exit positions. In previous studies [3–5] we observed formation of a high viscosity phase in the inlet, which is entrained into the contact forming a lubricating film and this supports observation in this work.

The link between β-sheet formation and wear has been indicated in this work. Generally, we find that 25BCS gives much thicker β-sheet deposits than HSF and this is associated with lower AWD. The presence of lipids appears to play an important role inhibiting β-sheet formation possibly through preferential interaction with the extended protein-form reducing cross-strand aggregation. Thus, although BCS appears to form abundant β-sheet fibrils in rubbing contacts this is reduced for HSF.

The work has shown very clearly the complexity of SF lubrication mechanisms and the influence of patient chemistry on wear and film

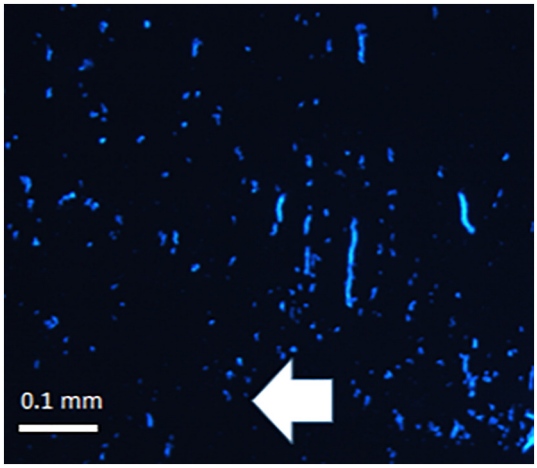

Fig. 12. ThT fluorescent images of fibril rolls formed by shearing 25BCS fluid between glass microscope slides. The primary direction of sliding is marked by the arrow.

formation. The question of a suitable model SF remains open, our work suggests that for most patient chemistries bench tests with 25BCS underestimate CoCrMo wear. The addition of a phospholipid component would be a starting point in developing a more relevant fluid. The research also raises the possibility of developing a more tailored approach to implant choice (design, materials etc) based on an assessment of patient SF chemistry, joint physiology and activity levels. However, it is recognised the current work is restricted to a very limited number of patients and this must be increased to obtain a more comprehensive understanding of these factors. NMR analysis of synovial fluid samples is still ongoing by the Musculoskeletal team and once this is completed, we will be able to develop a more complete awareness of the effects of protein/lipid chemistry on wear and risk of implant failure. Finally, we consider this approach could also be extended to other implant materials, both existing and in the development of new materials and combinations.

5. Conclusions

Residual surface films formed by 25BCS and HSF during CoCrMo wear tests were examined to understand the properties of the films and their role in the lubrication process. We conclude the following:

1. In bench tests HSF gives generally higher AWD (up to 77% increase), compared to 25BCS which is the standard implant wear screening lubricant.
2. During sliding protein-rich deposits are formed in and around the wear scar. For some HSF samples lipids were also detected in these deposits.
3. SF proteins denature due to shear in the confined gap geometry close to the contact zone. The denatured proteins form insoluble aggregates which precipitate onto the metal surfaces and, if formed in the inlet, are entrained into the contact contributing to a lubricating film.
4. Micro-IRRAS analysis indicates the aggregates have increased non-native β-sheet content.
5. ThT fluorescence imaging confirms the formation of non-native β-sheet aggregates with an amyloid-type fibril structure.

Conflict of interest

The authors have no conflicts of interest to declare.

Human ethics and consent

The work was carried out under human ethics REC reference 15/LO/0388 and patient consent was obtained for all human sample testing.

Acknowledgements

The authors wish to thank Professor J. Lindon and Dr. C. Boulange (Computational and Systems Medicine Imperial College London) for their contribution to the research project, Dr. H. Williams and Dr. R. Bhattacharya for setting up the biobank and sample collection and to the UK EPSRC for financial support of Ms. Stevenson (EP/M506345/1).

References

[1] D. Dowson, Z.M. Jin, Metal-on-metal hip joint tribology, Proc. Inst. Mech. Eng. H J. Eng. Med. 220 (2006) 107–118.
[2] V. Saikko, T. Ahlroos, Phospholipids as boundary lubricants in wear tests of prosthetic joint materials, Wear 207 (1997) 86–91.
[3] C. Myant, R. Underwood, J. Fan, P.M. Cann, Lubrication of metal-on-metal hip joints: the effect of protein content and load on film formation and wear, J. Mech. Behav. Biomed. Mater. 6 (2012) 30–40.
[4] J. Fan, C. Myant, R. Underwood, P. Cann, Synovial fluid lubrication of artificial joints: protein film formation and composition, Faraday Discuss. 56 (2012) 69–85.
[5] J. Fan, C.W. Myant, R. Underwood, P.M. Cann, A. Hart, Inlet protein aggregation: a new mechanism for lubricating film formation with model synovial fluids, Proc. Inst. Mech. Eng. H J. Eng. Med. 225 (2011) 696–709.
[6] D. Nečas, M. Vrbka, F. Urban, I. Křupka, M. Hartl, The effect of lubricant constituents on lubrication mechanisms in hip joint replacements, J. Mech. Behav. Biomed. Mater. 55 (2016) 295–307.
[7] D. Nečas, M. Vrbka, I. Křupka, M. Hartl, A. Galandáková, Lubrication within hip replacements–implication for ceramic-on-hard bearing couples, J. Mech. Behav. Biomed. Mater. 61 (2016) 371–383.
[8] T. Kitano, G.A. Ateshian, V.C. Mow, Y. Kadoya, Y. Yamano, Constituents and pH changes in protein rich hyaluronan solution affect the biotribological properties of artificial articular joints, J. Biomech. 34 (2001) 1031–1037.
[9] M. Roba, M. Naka, E. Gautier, N.D. Spencer, R. Crockett, The adsorption and lubrication behavior of synovial fluid proteins and glycoproteins on the bearing-surface materials of hip replacements, Biomaterials 30 (2009) 2072–2078.
[10] L.R. Gale, Y. Chen, B.A. Hills, R. Crawford, Boundary lubrication of joints characterization of surface-active phospholipids found on retrieved implants, Acta Orthop. 78 (2007) 309–314.
[11] B. Purbach, B.A. Hills, B.M. Wroblewski, Surface-active phospholipid in total hip arthroplasty, J. Orthop. Res. 396 (2002) 115–118.
[12] M.A. Wimmer, C. Sprecher, R. Hauert, G. Täger, A. Fischer, Tribochemical reaction on metal-on-metal hip joint bearings. A comparison between in-vitro and in-vivo results, Wear 255 (2003) 1007–1014.
[13] A. Wang, A. Essner, V.K. Polineni, C. Stark, J.H. Dumbleton, Lubrication and wear of ultra-high molecular weight polyethylene in total joint replacements, Tribiol. Int. 31 (1998) 17–33.
[14] M.A. Wimmer, J. Loos, R. Nassutt, M. Heitkemper, A. Fischer, The acting wear mechanisms on metal-on-metal hip joint bearings: in vitro results, Wear 250 (2001) 129–139.
[15] Y. Liao, R. Pourzal, M.A. Wimmer, J.J. Jacobs, A. Fischer, L.D. Marks, Graphitic tribological layers in metal-on-metal hip replacements, Science 334 (2011) 1687–1690.
[16] K.A. De Smet, C. Van Der Straeten, M. Van Orsouw, R. Doubi, K. Backers, G. Grammatopoulos, Revisions of metal-on-metal hip resurfacing: lessons learned and improved outcome, Orthopedic Clin. 6 (2011) 259–269.
[17] H. Stevenson, M. Parkes, L. Austin, M. Jaggard, P. Akhbari, U. Vaghela, H. Williams, C. Gupte, P. Cann, The development of a small-scale Wear test for CoCrMo specimens with human synovial fluid, Biotribology 1 (2018) 1–10.
[18] P. Cann, The "leaves on the line" problem-a study of leaf residue film formation and lubricity under laboratory test conditions, Tribol. Lett. 24 (2006) 151–158.
[19] J. Kong, S. Yu, Fourier transform infrared spectroscopic analysis of protein secondary structures, Acta Biochim. Biophys. Sin. 39 (2007) 549–559.
[20] H. LeVine III, Thioflavine T interaction with amyloid β-sheet structures, Amyloid 1 (1995) 1–6.
[21] M. Biancalana, S. Koide, Molecular mechanism of Thioflavin-T binding to amyloid fibrils, Biochim. Biophys. Acta 1804 (2010) 1405–1411.
[22] K.G. Malmosa, L.M. Blancas-Mejiac, B. Weberd, J. Buchnerd, M. Ramirez-Alvaradoc, H. Naikie, D. Otzena, ThT 101: a primer on the use of thioflavin T to investigate amyloid formation, Amyloid 24 (2017) 1–16.
[23] B. Bolognesi, G.G. Tartaglia, Physicochemical principles of protein aggregation, Prog. Mol. Biol. Transl. Sci. 3 (2013) 53–72.
[24] R.N. Rambaran, L.C. Serpel, Amyloid fibrils. Abnormal protein assembly, Prion. 2 (3) (2008) 112–117.
[25] D.M. Byler, H. Susi, Examination of the secondary structure of proteins by deconvoluted FTIR spectra, Biopolymers 25 (1986) 469–487.
[26] M. Jackson, H.H. Mantsch, The use and misuse of FTIR spectroscopy in the

determination of protein structure, Crit. Rev. Biochem. Mol. Biol. 30 (1995) 95–120.
[27] A. Barth, Infrared spectroscopy of proteins, Biochim. et Biophys. Acta (BBA)-Bioenergetics. 1767 (2007) 1073–1101.
[28] N.V. Venkataraman, S. Vasudevan, Characterization of alkyl chain conformation in an intercalated cationic lipid bilayer by IR spectroscopy, J. Phys. Chem. B 106 (2002) 7766–7773.
[29] V.I. Stsiapura, A.A. Maskevich, V.A. Kuzmitsky, V.N. Uversky, I.M. Kuznetsova, K.K. Turoverov, Thioflavin T as a molecular rotor: fluorescent properties of thioflavin T in solvents with different viscosity, J. Phys. Chem. B 112 (2008) 15893–15902.
[30] R. Harvey, D.R. Ferrier, Biochemistry, 5th ed., Wolters Kluwer Health/Lippincott Williams & Wilkins, Philadelphia, PA, London, 2011 International ed., Lippincott's illustrated reviews).
[31] E. Cerf, R. Sarroukh, S. Tamamizu-Kato, L. Breydo, S. Declaye, Y.F. Dufrénes, V. Narayanaswami, E. Goormaghtigh, J.-M. Ruysschaert, V. Raussens, Antiparallel β-sheet: a signature structure of the oligomeric amyloid β-peptide, Biochem. J. 421 (2009) 415–423.
[32] G. Zandomeneghi, M.R.H. Krebs, M.G. McCammon, M. Fändrich, FTIR reveals structural differences between native β-sheet proteins and amyloid fibrils, Protein Sci. 13 (2004) 3314–3321.
[33] O.S. Makin, L.C. Serpell, Structures for amyloid fibrils, FEBS J. 272 (2005) 5950–5961.
[34] D. Ami, F. Lavatelli, P. Rognoni, G. Palladini, S. Raimondi, S. Giorgetti, L. Monti, S.M. Doglia, A. Natello, G. Merlinie, In situ characterisation of protein aggregates in human tissues affected by light chain amyloidosis: a FTIR micro-spectroscopy study, Sci. Rep. 6 (2016) 29096.
[35] Y. Zou, Y. Li, W. Hao, X. Hu, G. Ma, Parallel β-sheet fibril and antiparallel β-sheet oligomer: new insights into amyloid formation of hen egg white lysozyme under heat and acidic condition from FTIR spectroscopy, J. Phys. Chem. B 117 (2013) 4003–4013.
[36] D.E. Barlow, G.H. Dickinson, B. Orihuela, J.L. Kulp III, D. Rittschof, K.J. Wahl, Characterization of the adhesive plaque of the barnacle Balanus amphitrite: amyloid-like nanofibrils are a major component, Langmuir 26 (2010) 6549–6556.
[37] A.L. Fink, Protein aggregation: folding aggregates, inclusion bodies and amyloid, Fold. Des. 3 (1998) R9–R23.
[38] E.K. Hill, B. Krebs, D.G. Goodall, G. Howlett, D.E. Dunstan, Shear flow induces amyloid fibril formation, Biomacromol. 7 (2006) 10–13.
[39] D.E. Dunstan, P. Hamilton-Brown, P. Asimakis, W. Ducker, J. Bertolini, Shear flow promotes amyloid-β fibrilization, Protein Eng. Des. Select. 22 (2009) 741–746.
[40] D.E. Dunstan, P. Hamilton-Brown, P. Asimakis, W. Ducker, J. Bertolini, Shear-induced structure and mechanics of β-lactoglobulin amyloid fibrils, Soft Matter 5 (2009) 5020–5028.
[41] P.B. Stathopulos, G.A. Scholz, Y.M. Hwang, J.A. Rumfeldt, J.R. Lepock, E.M. Meiering, Sonication of proteins causes formation of aggregates that resemble amyloid, Protein Sci. 13 (2004) 3017–3027.
[42] V. Vetri, C. Canale, A. Relini, F. Librizzi, V. Militello, A. Gliozzi, Maurizio Leone, M. Amyloid fibrils formation and amorphous aggregation in concanavalin A, Biophys. Chem. 125 (2007) 184–190.
[43] J. Fang, X. Zhang, Y. Cai, Y. Wei, Small globular protein motif forms particulate hydrogel under various pH conditions, Biomacromolecules 12 (2011) 1578–1584.